J. Fluid Mech. (2012), *vol.* 705, *pp.* 322–347.
doi:10.1017/jfm.2011.55

A dynamical instability due to fluid–wall coupling lowers the transition Reynolds number in the flow through a flexible tube

M. K. S. Verma and V. Kumaran†

Department of Chemical Engineering, Indian Institute of Science, Bangalore 560 012, India

(Received 8 April 2010; revised 28 November 2010; accepted 31 January 2011;
first published online 2 August 2011)

A flow-induced instability in a tube with flexible walls is studied experimentally. Tubes of diameter 0.8 and 1.2 mm are cast in polydimethylsiloxane (PDMS) polymer gels, and the catalyst concentration in these gels is varied to obtain shear modulus in the range 17–550 kPa. A pressure drop between the inlet and outlet of the tube is used to drive fluid flow, and the friction factor f is measured as a function of the Reynolds number Re. From these measurements, it is found that the laminar flow becomes unstable, and there is a transition to a more complicated flow profile, for Reynolds numbers as low as 500 for the softest gels used here. The nature of the f–Re curves is also qualitatively different from that in the flow past rigid tubes; in contrast to the discontinuous increase in the friction factor at transition in a rigid tube, it is found that there is a continuous increase in the friction factor from the laminar value of $16/Re$ in a flexible tube. The onset of transition is also detected by a dye-stream method, where a stream of dye is injected into the centre of the tube. It is found that there is a continuous increase of the amplitude of perturbations at the onset of transition in a flexible tube, in contrast to the abrupt disruption of the dye stream at transition in a rigid tube. There are oscillations in the wall of the tube at the onset of transition, which is detected from the laser scattering off the walls of the tube. This indicates that the coupling between the fluid stresses and the elastic stresses in the wall results in an instability of the laminar flow.

Key words: flow-vessel interactions, instability

1. Introduction

The transition from a laminar to a turbulent flow in a pipe, at a Reynolds number of ∼2100, discovered by Reynolds (1893) more than a century ago, has significant technological implications. The drag force in the turbulent flow is significantly larger than that in a laminar flow for a fixed flow rate, because the momentum transport across the flow by the turbulent fluctuations is much larger than that by molecular diffusion in a laminar flow. This results in a significantly larger pressure drop for a given flow rate. The transport coefficients for mass and heat transfer in a turbulent flow are also significantly higher than those in a laminar flow, owing to the greater efficiency of mixing by the turbulent eddies. The laminar–turbulent transition in a pipe

† Email address for correspondence: kumaran@chemeng.iisc.ernet.in

flow continues to be a poorly understood phenomenon more than a century after it was discovered (Hof, Juel & Mullin 2003; Kerswell 2005; Hof *et al.* 2006). In contrast to other well-studied flow instabilities, such as the Taylor–Couette and Rayleigh–Benard instabilities (Chandrasekhar 1981; Drazin & Reid 1981), the transition is not triggered by a linear instability of the base flow to infinitesimal perturbations. The fully developed laminar pipe flow is linearly stable at all Reynolds numbers. Experimentally, the flow can be maintained in the laminar regime at Reynolds numbers as high as 10^5, provided care is taken to ensure that there are no disturbances in the experimental set-up. The transition in rigid pipes appears to be due to an instability to finite-amplitude perturbations.

In microfluidic applications, it is desirable to induce a transition to increase the mixing rates. In tubes of submillimetre sizes, the flow is usually in the laminar regime, since the channel width or tube diameter is small. In a laminar flow with smooth streamlines, mixing occurs only by molecular diffusion, which is much slower than turbulent diffusion. Therefore, one encounters the engineering limitation that the rates of mass and heat transfer are much slower than those in a turbulent flow. Several strategies have been proposed for enhancing the mixing rates, including patterning grooves in channel walls (Stroock *et al.* 2002), electro-osmotic flows (Bazant & Squires 2004), multiple bends and converging sections, etc. One method for inducing an instability is to replace the rigid walls of the microtube with a sufficiently soft material (Kumaran 2003). The instability due to flexible walls has been theoretically well studied, but it is fair to say that there is not, as yet, any experimental evidence for the applicability in real systems.

There have been several theoretical studies on the stability of the flow past flexible surfaces, both at low and high Reynolds numbers. Even in the absence of inertia (zero Reynolds number), there is an instability when the dimensionless number $V\eta/GR$ increases beyond a critical value (Kumaran, Fredrickson & Pincus 1994; Kumaran 1995). Here, V is the characteristic flow velocity, η is the fluid viscosity, G is the shear modulus of the elastic material and R is the characteristic length scale. The mechanism of instability is the transfer of energy from the mean flow to the fluctuations due to the shear work done at the interface. The zero Reynolds number instability is sensitive to the type of wall used, and to the specific constitutive relation for the wall material. Flows past membranes of infinitesimal thickness are always stable (Thaokar, Shankar & Kumaran 2001). There is an instability for the flow past soft solids of finite thickness, but the transition depends on the type of constitutive relation (linear or neo-Hookean) used for the solid (Chokshi & Kumaran 2008). This instability turns out to be subcritical in most cases, similar to the laminar–turbulent transition in a channel flow (Chokshi & Kumaran 2008). This implies that the flow does not transition smoothly into a post-transition periodic state, and so it is not useful for generating non-laminar flows with controlled mixing characteristics. For the flow through deformable tubes, there is an instability when the linear elastic model is used for the wall constitutive relation, but this is not present when the neo-Hookean model is used (Gaurav & Shankar 2009). In contrast, for the Couette flow past a flexible surface, the flow past a neo-Hookean surface is more unstable than that past a surface described by the linear elastic model. This indicates that an accurate wall elasticity model is necessary for predicting the low Reynolds number instability.

The zero Reynolds number instability of the flow past a flexible surface has been verified experimentally, and quantitative agreement between theory and experiments were obtained for this instability (Kumaran & Muralikrishnan 2000; Muralikrishnan & Kumaran 2002). These studies also suggested that the instability is subcritical because

the authors were unable to maintain the system in a non-laminar oscillatory state after the onset of the instability. More detailed experiments were carried out by Eggert & Kumar (2004), who managed to capture both hysteric behaviour in the variation of viscosity with strain rate, as well as oscillatory variation of viscosity with time at a constant strain rate. The power spectra of the variation of the viscosity with time were calculated, and the authors were able to determine that the dominant frequency corresponds to a time period larger than the period of rotation of the rheometer. The nature of the transition is found to be subcritical in all cases, in agreement with the theoretical predictions (Shankar & Kumaran 2001*b*; Chokshi & Kumaran 2008). It has further been shown by Shrivastava, Cussler & Kumar (2008) that the elastohydrodynamic instability at the interface could significantly enhance the mass transfer at the surface by $\sim$25 %, thereby making it feasible for enhancing transport rates in microfluidic applications.

However, it is difficult to utilize this for real microfluidic systems, owing to the high fluid velocity and viscosity required. The velocity required for destabilizing the flow is proportional to (GR/η), where G is the shear modulus, η is the fluid viscosity and R is the tube radius. However, there is the additional constraint that in the low Reynolds number limit, the velocity has to be much smaller than $(\eta/\rho R)$, where ρ is the fluid density. Therefore, this instability can only be realized in the regime $\Sigma = (\rho GR^2/\eta^2) \ll 1$. This requires a very low shear modulus and high shear viscosity. The softest materials that can be fabricated have a shear modulus of $\sim$1 kPa, and so the low Reynolds number instability can only be realized for very viscous fluids with viscosity between 1 and 100 kg m^{-1} s^{-1} (between 10^3 and 10^5 times the viscosity of water) for a tube radius in the range 100 μm–1 mm. This explains the use of high viscosity silicone oil ($\eta = 1$ kg m^{-1} s^{-1}) in the experiments (Kumaran & Muralikrishnan 2000; Muralikrishnan & Kumaran 2002) for verifying the low Reynolds number instability. The need for very high fluid viscosity, and the resultant large pressure drop, also makes this mechanism infeasible for enhancing mixing in microfluidic applications.

In the high Reynolds number regime, there have been two other mechanisms of instability for the flow past a flexible surface, which are qualitatively different from the instability for the flow past a rigid surface. The first is the 'inviscid' instability in the high Reynolds number limit (Kumaran 1996; Shankar & Kumaran 1999, 2000), where the viscous effects are negligible in the bulk of the flow, although they are important in boundary layers of thickness $Re^{-1/2}$ at the walls. The transition takes place due to an internal critical layer of thickness $Re^{-1/3}$ within the flow, where the wave speed is equal to the flow velocity. The transition Reynolds number follows the scaling $Re_t \propto \Sigma^{1/2}$, where $\Sigma = (\rho GR^2/\eta^2)$ is a dimensionless number which depends only on the material properties and geometry, but not on the flow velocity. The transition is due to the destabilizing effect of inertial stresses within the bulk of the flow. The second high Reynolds number instability, which is qualitatively different from the instability in the flow past rigid surfaces, is the 'wall mode' instability (Kumaran 1998*a*; Shankar & Kumaran 2001*a*, 2002). Although this instability occurs at high Reynolds number, the destabilizing mechanism is the same as that for the viscous instability, which is the transfer of energy from the mean flow to the fluctuations due to the shear work done at the interface. Here, the viscous stresses are confined to a boundary layer of thickness $Re^{-1/3}$ at the wall of the channel, and the transition Reynolds number scales as $Re_t \propto \Sigma^{3/4}$. Recent work has indicated that the transition is not very sensitive to the constitutive relation used for the wall material, and there is little difference between the transition predicted for a linear and neo-Hookean solids.

In addition, the transition is predicted to be super-critical (Chokshi & Kumaran 2009). This implies that the system transitions into a well-defined periodic state, in which there are wall oscillations. This instability could be used to enhance mixing, and to increase the rates of mass and heat transfer.

These high Reynolds number instabilities may be considered more feasible for triggering an instability in microfluidic applications, because they occur in the regime $\Sigma \gg 1$ for low viscosity fluids. However, careful numerical calculations (Shankar & Kumaran 2002) show that this is still difficult to realize in practice. For tubes of diameter 100 μm–1 mm, soft wall materials with $G = 1$ kPa and for a fluid with the viscosity of water (10^{-3} kg m^{-1} s^{-1}), the parameter $\Sigma = (\rho G R^2/\eta^2)$ is in the range 10^6–10^8. The theoretical transition Reynolds number is $\sim 6 \times 10^3$ at $\Sigma = 10^6$, and $\sim 3.2 \times 10^4$ at $\Sigma = 10^7$. This is much higher than the rigid-tube transition Reynolds number of 2100, and so this mechanism was considered infeasible for inducing mixing in microfluidic applications.

There have been previous experimental studies (Krindel & Silberberg 1979) which reported, based on flow rate measurements, that the drag force in a flexible-walled tube is higher than the laminar value for a rigid tube. However, the authors were not able to carefully control the elasticity modulus of the wall material. A subsequent study Yang *et al.* (2000) concluded that the higher drag force in the Krindel and Silberberg experiments is due to the slow convergence of streamlines, and not due to an instability of the base laminar flow. In order to definitively establish the onset of an instability, it is necessary to simultaneously detect the instability in the fluid flow and the onset of wall oscillations. The flow instability can be detected by the dye-stream method of Reynolds (1893) or from the pressure gradient as a function of the flow rate (Krindel & Silberberg 1979). However, the absence of a quantitative method for the detection of wall oscillation results makes it difficult to conclusively infer an instability of the flow. This is complicated by the deformation of a soft tube due to an applied pressure gradient, and the concern that the change in the friction factor could be due to tube deformation alone. Further, the frequency of oscillations at transition is predicted to be in the range 200–500 Hz (Shankar & Kumaran 2002). Such large frequencies cannot be detected by ordinary cameras filming at 30 frames s^{-1}, and it is necessary to use a high-speed camera connected to a microscope to detect an instability using the dye-stream method.

Here, we report the experimental realization of a flow instability in tubes with elastic walls, coupled with the simultaneous observation of wall motion. The material used for the walls is soft polydimethylsiloxane (PDMS), in which the concentrations of the constituents have been modified to achieve a shear modulus as low as 17 kPa. It is shown that the transition Reynolds number is lower than that of the flow past a rigid surface, and we have been able to achieve a minimum transition Reynolds number of ∼500 in the experiments. It is also shown that, as predicted theoretically, the nature of the transition is different from that in rigid-walled tubes. The transition in a rigid tube is accompanied by a discontinuous change in the friction factor, which is the ratio of the wall shear stress and the kinetic energy per unit volume of the flow. This is because transition to turbulence is due to finite-amplitude fluctuations, with amplitude greater than a minimum value. In contrast, the wall mode instability for the flow past a flexible surface is a linear instability, to infinitesimal perturbations, and should be accompanied by a continuous increase in the friction factor at the transition point according to theoretical predictions. This continuous transition is confirmed by the experiments.

In addition to the transition Reynolds number, theoretical studies using a weakly nonlinear analysis have also shown that the initial bifurcation is supercritical for the wall-mode instability. In the experiments, this has been verified by measuring the variation of the friction factor after transition. In the laminar flow past both rigid and flexible surfaces, the friction factor decreases as $16/Re$ before transition. After transition, the friction factor in a rigid tube decreases more slowly, and approaches a constant value in the limit of high Reynolds number. In contrast, we find in the experiments that for the flow in a flexible tube, the friction factor actually increases with Reynolds number in the high Reynolds number limit, and the increase is continuous, indicating that the bifurcation is supercritical.

2. Experimental methods

2.1. *Fabrication techniques*

The microtubes were fabricated in blocks of cross-linked PDMS (Sylgard 184, Dow Corning) using a slender glass monofilament of diameter 800–1200 μm and length 220 mm with the templates as shown in figure 1 (Verma, Majumder & Ghatak 2006). Since we would like to study the stability of a fully developed flow, it is necessary to ensure that the flow is laminar at the entrance of the tube. For this, a development section tube is made of hard PDMS with 3 % catalyst concentration (shear modulus $G' = 86.4$ kPa) upstream of the test section made of the soft gel, as shown in figure 1. Two different lengths, ∼4.5 and 10 cm, were used for the development section, in order to verify that the development length used here does not affect the results. After the development section, the test section of ∼10 cm in length is cast adjacent to the development section. The procedure used is as shown in figure 1. For the development section, a rectangular channel formed by the bottom glass plate, and two side plates and a top glass plate, in which a glass monofilament of the desired diameter is held in place by sticky tape. All of the glass plates were covered with polyester sheets to prevent the polymer from sticking to the glass. The channel and monofilament are held with the axis of the monofilament vertical, and the prepolymer and catalyst mixture are poured in. After curing the mixture at 80 °C, the upper glass wall is removed, and another (test) section of length ∼10 cm is adjacent to the development section using the same side glass plates, but with the axis of the monomer filament horizontal. Prepolymer and catalyst of the desired concentration for the test section are mixed, filled into the rectangular channel adjoining the development section and around the same glass filament, and then cured. After both sections are cured, these are swelled in the solvent toluene (Lee, Park & Whitesides 2003), and the monofilament is removed leaving a tubular bore in the gel block. The gel is then deswelled at 10–15 °C in a homogeneous manner to avoid cracks. This gives a tubular bore in which the walls of the development section have a catalyst concentration of 3 % ($G' = 86.4$ kPa), while the test section has a lower catalyst concentration and shear modulus. After this, a hole is punched in the side of tube with a sharp-edged needle for the pressure sensor, as depicted in figure 1(*g*). The excess material is removed from the hole using tweezers, so that there is no blockage or constriction in the tube at the connection for the pressure sensor.

A sample of the tube fabricated in this manner is shown in figure 2(*a*). In order to verify the smoothness of the walls of the tube, scanning electron microscopy (SEM) images of the tube were taken after completing the experiments. The tubes were sliced along the axis, and SEM images were taken of the wall of the tube. These images (figure 3) show that the wall is smooth down to the micrometre scale.

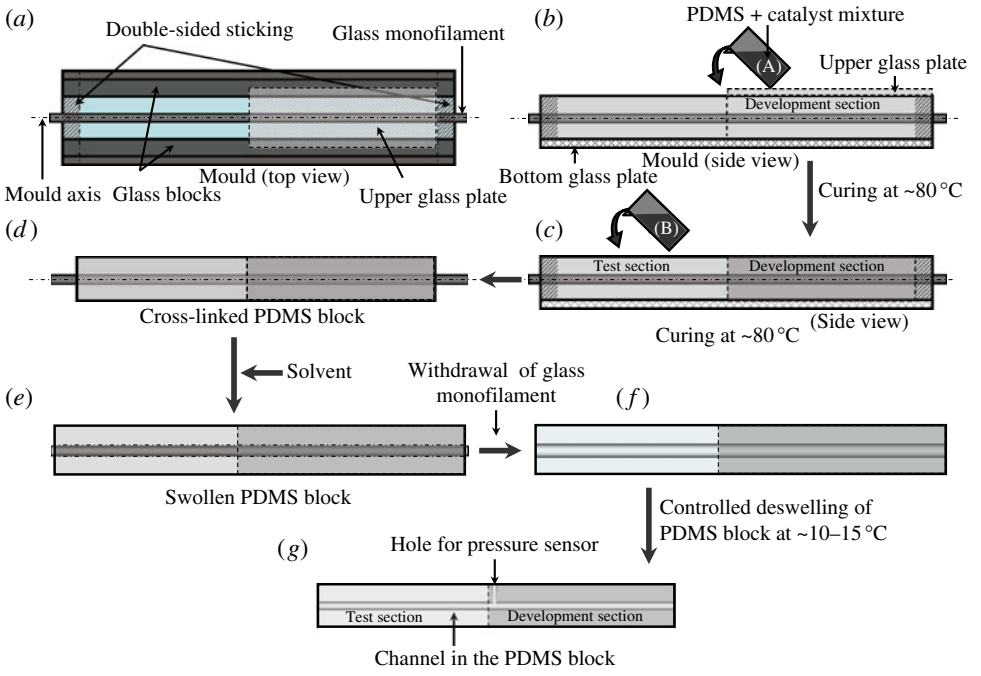

FIGURE 1. Fabrication procedure: (*a*) glass mould with side and bottom glass plates, and with a top glass plate covering one half of the channel and microfilament held in place by sticky tape; (*b*) channel held with axis vertical and prepolymer and catalyst mixture *A* for the development section (catalyst concentration 3 %) poured into one half of the channel; (*c*) development section cured, channel is held horizontal and prepolymer and catalyst mixture *B* for the test section is poured into the other half of the channel; (*d*) test section cured and the surrounding glass plates removed; (*e*) channel swollen in organic solvent and glass microfilament removed; followed by (*f*) controlled deswelling at low temperature to avoid cracks; and (*g*) hole punched in wall of channel in the hard development section just upstream of the joint for pressure transducer.

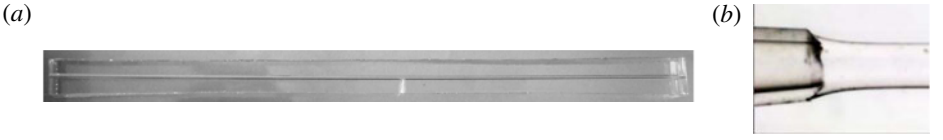

FIGURE 2. Image of the tube (*a*), and the deformation of the gel tube around the micropipette tip at the inlet of the hard development section of the PDMS block (*b*). In (*a*), the inlet is on the left, the outlet on the right and the pressure port in the centre for tubes with diameter 1200 μm. The soft test section of length ∼10 cm on the right is made with soft gel, and the hard development section of length ∼10.5 cm on the left is made with hard gel. The pressure port is ∼2 mm upstream of the joint between the test and development sections.

The development and test sections are joined seamlessly by a covalent linking of the monomers in the two sections, and the joint is strong enough that it does not split even for the highest pressure drops used here. The casting is done in such a way that there are no irregularities in the tube between the development and the test section. SEM images of the joint between the development and test sections (figure 4) show that the

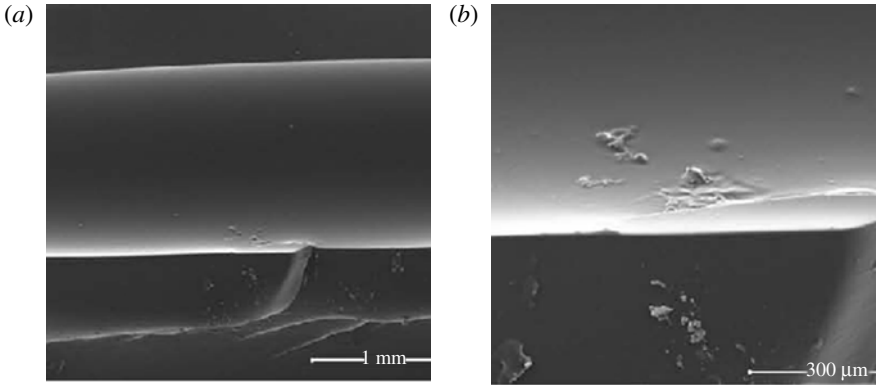

FIGURE 3. SEM images of the PDMS tube (*a*) inside surface and (*b*) the tube surface at higher magnification.

joints are completely smooth, except for a few features of dimension 2–3 μm. In order to verify that the joint between the development section and the test section does not influence the flow, all of the tubes, including the hard tubes with catalyst concentration 3 % ($G' = 86.4$ kPa), were fabricated in a two-step procedure as discussed before in the fabrication techniques. This enables us to verify that the presence of the joint does not affect the flow characteristics in a rigid-walled tube.

The measurement of the shear moduli of the PDMS is discussed below. While discussing the fabrication, the tubes can be classified into two types, depending on their hardness. When the catalyst concentration is greater than 3 %, the hardness of the walls is sufficiently large that we do not observe a decrease in the transition Reynolds number below 2100. We use a gel with catalyst concentration of 3 % ($G' = 86.4$ kPa) or greater as a control, to verify that we obtain the rigid-walled tube results in the present set-up if the tube walls are made sufficiently hard. The second type is for catalyst concentrations less than ∼3 %, where we observe that the transition Reynolds number is lower than that for the flow through a rigid tube.

For measuring the pressure drop in the test section, a pressure transducer, model PDCR 810 (Druck Limited), is connected to the pressure port in the development section, ∼2 mm upstream of the test section, where the gel is hard enough that the pressure transducer can be inserted without leakage. One end of the tube is connected to a pressurized liquid vessel, discussed a little later, using a tapered conical microtip (TORSONS 2–200 μl) connector which is used in micropipettes. In order to ensure a seamless connection between the microtip and the tube in the PDMS block, the end of the microtip, which is tapered at an angle of 6°, is cut to obtain a diameter as close as possible to that of the diameter as that of the tube. There is a small amount of deformation of the tube around the tip, and this deformation provides a tight fit which prevents any leakage at the joint between the microtip and the tube, as shown in figure 2(*b*).

2.2. *Characterization of the PDMS gel*

The shear and compression moduli of the PDMS gel were measured using an AR1000-N rheometer using a parallel-plate configuration. This consists of a stationary bottom plate and a rotating top plate (geometry) of diameter 4 cm.

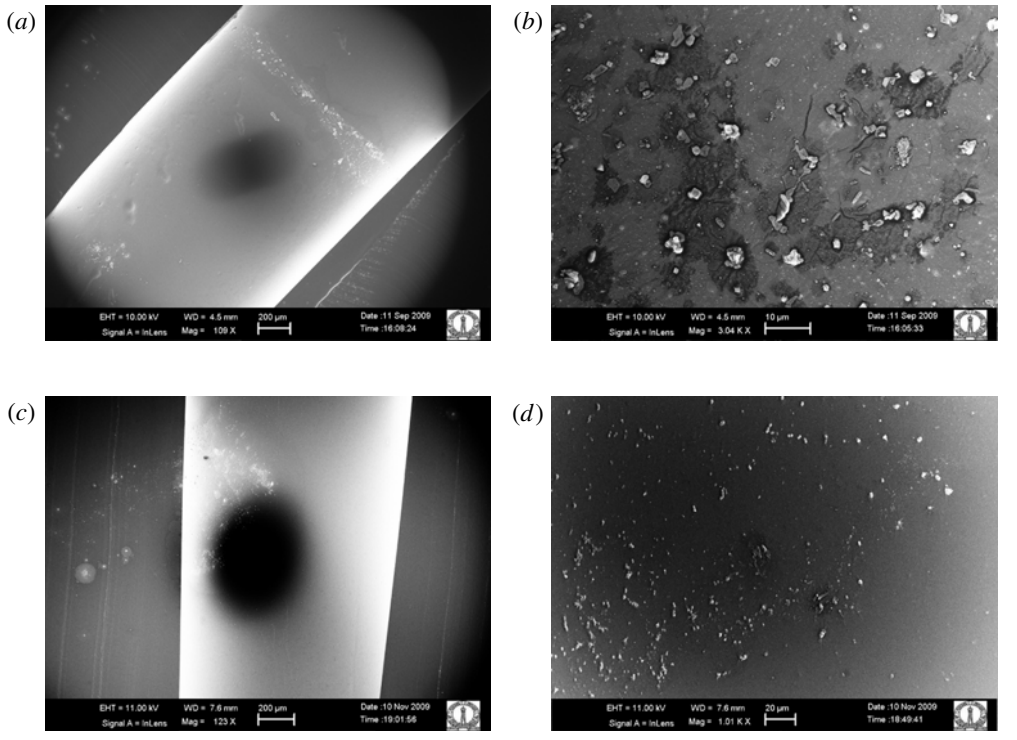

FIGURE 4. SEM images of joint between the development and test sections in a PDMS tube. Panels (*a*) and (*b*) show the joint between a development section made with 3 % catalyst concentration ($G' = 86.4$ kPa) and a test section made with 1.75 % catalyst concentration ($G' = 17.5$ kPa) at different magnifications, while (*c*) and (*d*) show the joint between two sections made with 3 % catalyst concentration ($G' = 86.4$ kPa) at different magnifications. The dark shadow in the centre is due to the equipment, and is not a feature of the sample.

For this purpose, along with the PDMS block containing the tubular bore, an additional PDMS block of the same composition was cast in the shape of a disc of diameter 4 cm and thickness 2 mm, without any tube. The gel disc was placed on the bottom plate of the rheometer, and the top plate was lowered until it made contact with the gel surface. Contact was detected when the normal force on the bottom plate increased to 0.2 N, which is the default instrument setting for detecting contact. The rheometer was then operated in the oscillatory mode, where an oscillatory stress was applied on the top plate and the angular displacement was measured. The storage and loss modulus are calculated directly using the rheometer software assuming the deformation in the gap is affine. The frequency spectrum of a typical gel cast using the above concentrations is shown in figure 5 in the range 6.283–400 Hz. The storage modulus G' shows a distinct plateau region in the frequency range 100–400 Hz, and we call this the 'plateau modulus' for the gel. The loss modulus G'' does not show a linear dependence on the frequency in this range, but it does increase with frequency. The plateau modulus, which we define as the average of G' in the frequency range 100–400 Hz, is shown as a function of the concentration of the cross-linker in figure 6(*a*). The averages were calculated over four different samples prepared with the same concentration of catalyst and prepolymer. Figure 6(*a*) also shows error bars,

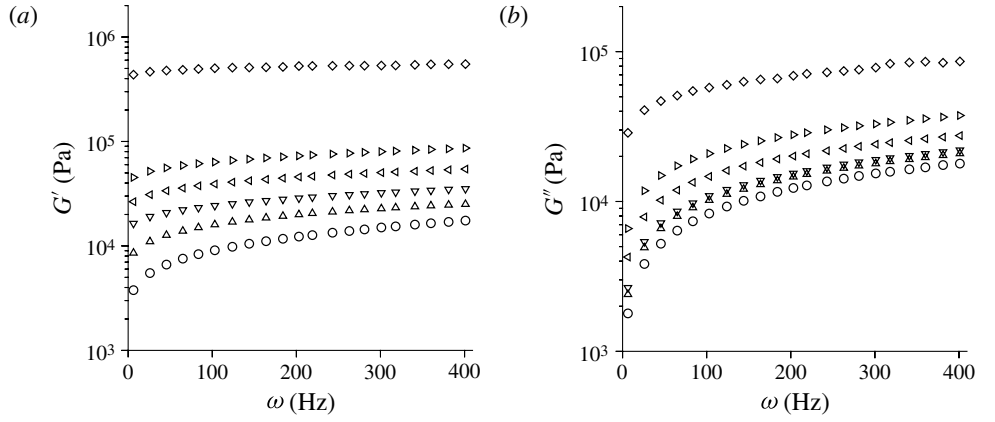

FIGURE 5. Storage modulus G' (a) and loss modulus G'' (b) as a function angular frequency ω for PDMS gels with different concentrations of the cross-linker, 1.75 % (○), 2 % (△), 2.25 % (▽), 2.5 % (◁), 3 % (▷), and 10 % (◇).

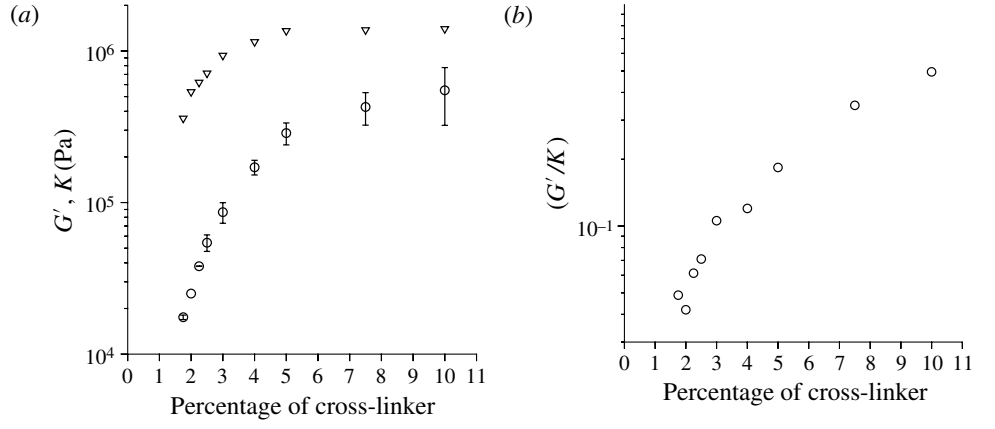

FIGURE 6. The shear (G', ○) and compression (K, ▽) moduli (a), and the ratio (G'/K) (b) as a function of the concentration of the cross-linker.

with length equal to two times the standard deviation over the four experimental measurements.

The compression modulus measurement was also made using the AR1000-N rheometer. For compression modulus measurement, the same top plate geometry of diameter 4 cm in the rheometer was used. The top plate was lowered until it came into contact with the PDMS disc. The top plate was further lowered in steps of 20 μm, and the normal force was recorded. The normal stress was calculated as the ratio of the normal force and the area of contact. The compression modulus K, which is the ratio of the normal stress and the normal strain, is also shown as a function of catalyst concentration in figure 6(a). It should be noted that the normal stress is measured under steady conditions, and not under oscillatory forcing. This is because the rheometer is not designed for oscillatory displacement perpendicular to the surface of the gel, and we were only able to measure the zero-frequency compression modulus. The compression modulus K is shown as a function of the cross-linker concentration

in figure 6(*a*). Since the variation in the compression modulus was very small in the experiments with different gel samples, the error bars for K have not been plotted in figure 6(*a*).

It should be noted that the modulus measured in the compression experiments is the volumetric compression modulus K, and not the Young's modulus E. This is because the thickness of the sample (2 mm) is much smaller than the diameter (4 cm). When the sample is compressed, it is also prevented from expanding laterally due to the frictional forces acting at the top and bottom surface. It has been verified experimentally that the amount of protrusion from the sides between the top and bottom plates is much smaller than the volume decrease due to the compression of the sample between the geometry and the bottom plate. Therefore, the modulus measured in the experiments is the volumetric compression modulus K. The ratio (G'/K) is shown as a function of catalyst concentration in figure 6(*b*). It is observed that the ratio of the compression and shear modulus is $O(1)$ at high catalyst concentrations when the material is hard, but it decreases to a very small value, of the order of 0.04, when the catalyst concentration decreases and the material becomes softer. This implies that the material becomes more incompressible (rubber-like) as the material becomes softer, since the stress required for shear deformation is small compared with that for compressional deformation.

The near-incompressible nature of the material is of significance, because most of the theoretical studies assume that the material is perfectly incompressible. In the theories, the dynamics of the solid material is described using a displacement field $\boldsymbol{u}$, which is the displacement of the material points from their equilibrium positions due to applied stresses. When the material is incompressible, the mass conservation equation reduces to the condition that the trace of the deformation tensor is zero. The stress tensor consists of an isotropic pressure to enforce incompressibility, in addition to the elastic and viscous components. The rheological measurements shown in figure 6(*b*) indicate that softer materials are more incompressible, in the sense that for equal magnitudes of bulk and shear stress, the ratio of bulk and shear deformation becomes smaller as the gel shear modulus decreases. In addition, as discussed earlier, the wall mode instability is relatively insensitive to the constitutive relations used for the wall material. This implies that the theoretical predictions should be directly comparable with the experimental results.

The surface roughness of the surface of the tubes was measured using a Wyko surface profiler, which uses a non-contact phase-shifting interferometry technique. Contact methods, such as atomic force microscopy (AFM) profiling, cannot be used for soft materials due to surface deformation that occurs under an applied force. In the phase-shifting interferometry technique, light of wavelength of around 640 nm is split using a beam splitter. One half is reflected from the test surface, while the other half is reflected from a reference surface. These two combine to form interference fringes, and the roughness of the surface is deduced from the variation of phase shift with position. This technique has a resolution of 160 nm for the surface height.

In order to measure the roughness, the tube was sliced in half lengthwise along its axis after the experiment, and the exposed half of the cylindrical surface was placed under the profiler beam. The beam was directly incident on the curved surface, and the roughness was measured. The area scanned for the surface roughness was of dimension 500 μm × 700 μm. The average roughness is calculated by averaging over four scans for each tube sample, and the standard deviation over these four independent readings is also calculated. These average roughness of the tube wall for gels with different shear moduli is provided in table 1. It should be noted that the

G' (kPa)	17.5	25.1	54.4	86.4
Average roughness	1.91	2.31	2.38	1.75
Standard deviation	0.51	0.25	0.69	0.82

TABLE 1. Roughness in micrometres for tube samples with different shear moduli.

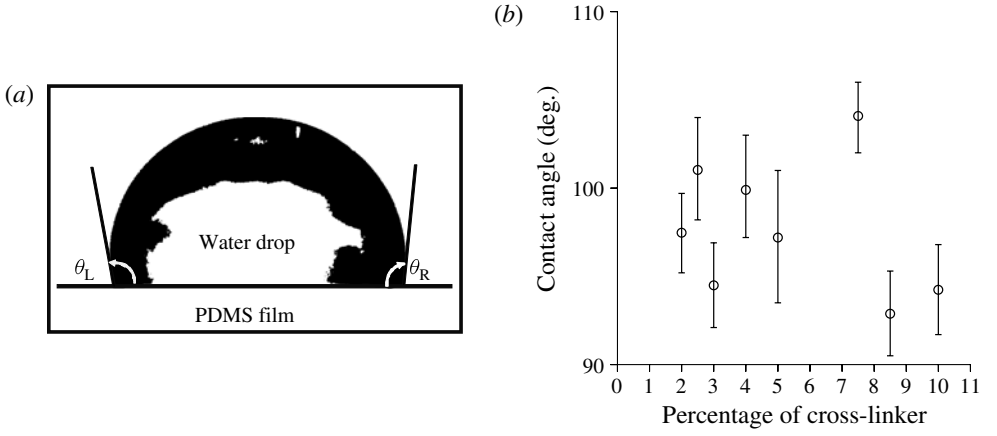

FIGURE 7. A representative image of a water droplet on the PDMS surface used for measuring the contact angle (*a*), and the contact angle for the water–PDMS interface as a function of the percentage of cross-linker (*b*).

surface of the tube is curved in our measurements. Since the width of the beam is 500 μm and the channel diameter is 1200 μm, the maximum slope of the surface from horizontal at the edge of the beam is ∼25°. Owing to this, the roughness measured will be underestimated by about ∼10 % at the edge of the curved surface, and we would expect an average underestimation of about ∼5 %. It is observed that the average roughness is only 1–2 μm for all of the tubes, in comparison with the tube diameter which is between 800 and 1200 μm. Thus, the ratio of the average roughness and tube diameter is 0.0025 or less in all of our experiments.

The contact angle measurements have been carried out between water and the PDMS gel, in order to determine whether the wetting properties change as the gel is made softer. A representative image for measuring the contact angle is shown in figure 7(*a*), where the contact angle on both the right and left sides of the droplet are measured, and the average is taken. The results for the variation of the contact angle with cross-linker concentration is shown in figure 7. The error bars are of length equal to two times the standard deviation obtained by taking four independent measurements on different gels with the same catalyst concentration. The results indicate that the contact angle is slightly larger than 90° in all cases, indicating that the gel surface is always hydrophobic. In addition, subject to the experimental error bars, there is no systematic variation in the contact angle as the catalyst concentration is decreased, or the gel is made softer.

2.3. *Experimental measurements*

Figure 8 shows a schematic of the experimental set-up for the measurement of pressure drop and flow rate, the dye-stream visualization and laser scattering off

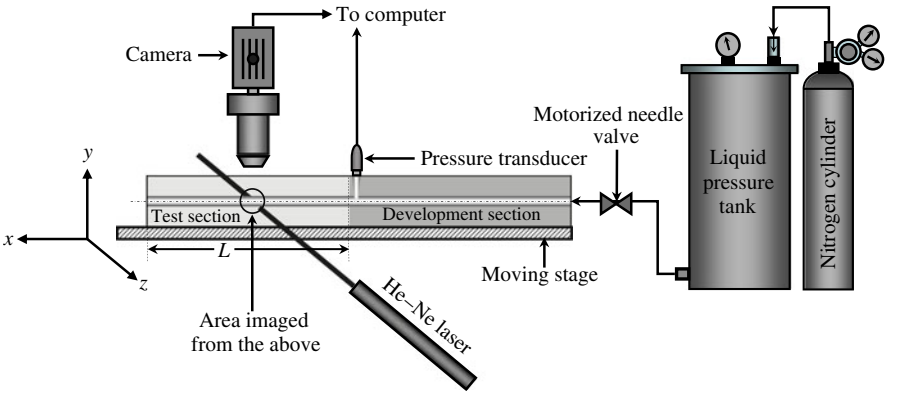

FIGURE 8. Schematic of the experimental set-up.

the tube walls in the flexible tube. The water is filled in a pressure tank of diameter 26 cm and height 70 cm, and is pressurized to 32 p.s.i. by connecting it to a nitrogen cylinder. The inlet of the sample tube is connected to the pressurized tank through a motorized needle valve and silicone tubing, as depicted in figure 8. The silicone tubing is connected to the inlet of the sample tube using a conical pipette tip as discussed earlier. The flow rate through the sample tube is controlled by the motorized needle valve, which is connected to a variable voltage power source.

The pressure transducer is connected to the sample tube in the development section as depicted in figure 8. A data acquisition card (NI USB-6009, National Instruments) is used to interface the pressure transducer with a computer in order to obtain pressure as a function of time. To measure the liquid flow rate through the sample tube, a 100 ml measuring cylinder is used and the fluid is collected at the outlet of the tube over periods ranging from 10 to 150 s, depending on the flow rate. The flow rate is calculated from the volume of fluid collected and the time interval.

When a pressure drop is applied across the tube, it is observed that there is a variation in the tube diameter along the length of the tube. In order to quantify this variation, a stereo microscope (MEIJI brand) attached to a webcam (Logitech QuickCam S5500) has been used to take images of the tube at different locations along the length (the x direction in figure 8). The optical axis of the microscope is along the y axis, which is perpendicular to the x axis, which is the axis of the tube. The entire tube and pressure transducer are mounted on a moving stage, so that the tube can be moved with respect to the microscope in order to take images along the entire length. The tube diameter at different downstream locations is measured using images from the microscope and camera. The diameter before applying the pressure drop, denoted by d_0, was approximately 1.2 mm; however, this was measured for each individual experiment since there is a slight variation of $\sim$10 % in the diameter in the casting process. The diameter was measured at seven downstream locations, $x = 0$, 1, 3.5, 4.75, 6, 7.75 and 9.5 cm, from the inlet of the test section (figure 8). The variation of diameter with position is shown in figure 9 for the softest gel with catalyst concentration 1.75 % ($G' = 17.5$ kPa) at different Reynolds numbers. Figure 9 clearly shows that there is a significant variation in the diameter along the length of the tube as the Reynolds number increases, but the maximum slope of the wall of the tube at the inlet is still small. The maximum slope is 0.01 at $Re = 451$, 0.042 at $Re = 951$, 0.051 at $Re = 1020$, 0.067 at $Re = 1140$, 0.088 at $Re = 1240$ and 0.141 at $Re = 1420$.

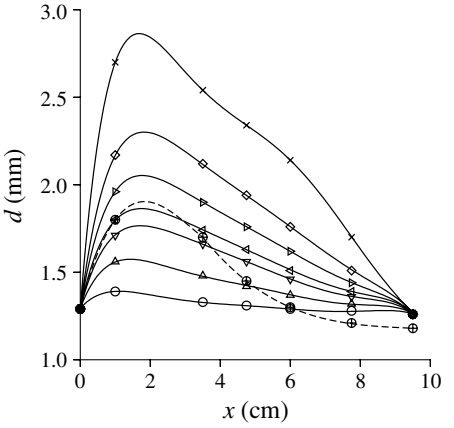

FIGURE 9. Tube diameter as a function of streamwise location for different Reynolds numbers, $Re = 451$ ($\circ$), $Re = 776$ ($\triangle$), $Re = 951$ (∇), $Re = 1020$ ($\triangleleft$), $Re = 1140$ ($\triangleright$), $Re = 1240$ ($\diamond$), $Re = 1420$ ($\times$), for a gel-walled tube with shear modulus $G' = 17.5$ kPa, catalyst 1.75 %. The symbol $\oplus$ and the dashed line show the variation of the diameter of a tube with varying diameter cast from hard PDMS gel with $G' = 0.550$ MPa, catalyst concentration 10 %.

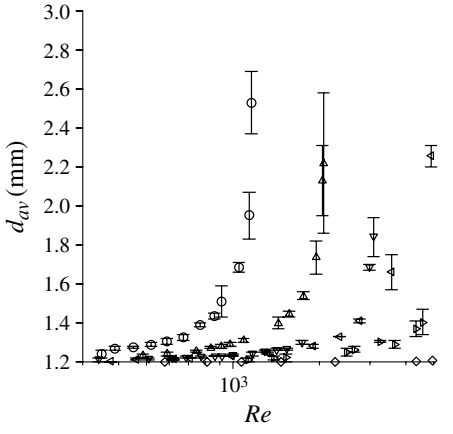

FIGURE 10. The average diameter d_{av} for a tube with diameter 1.2 mm before expansion. The shear modulus and catalyst concentration in the tubes are: $\circ$, $G' = 17.5$ kPa, catalyst 1.75 %; $\triangle$, $G' = 25.1$ kPa, catalyst 2 %; ∇, $G' = 38.0$ kPa, catalyst 2.25 %; $\triangleleft$, $G' = 54.4$ kPa, catalyst 2.5 %; $\triangleright$, $G' = 86.4$ kPa, catalyst 3 %; and $\diamond$, $G' = 0.55$ MPa, catalyst 10 %.

Since transition takes place at a Reynolds number of $\sim$940 for the softest gel with catalyst concentration 1.75 % ($G' = 17.5$ kPa), the maximum slope is $\sim$5 %. As we discuss later, the slope at the location in the converging section where we first observe an instability, which is $\sim$0.006, is smaller still. The average diameter (averaged over the entire length) of tubes of different shear moduli are shown as a function of Reynolds number in figure 10.

Using the high-pressure liquid tank and the motorized valve, a broad range of Reynolds numbers in the range 100–10 000 was achieved. Since the diameter and velocity of the fluid in the tube vary as a function of position, the average diameter

and velocity were used for calculating the Reynolds number. The friction factor is related to the flow rate and pressure drop for a cylindrical tube by,

$$f = \frac{\pi^2}{32}\frac{(\Delta p/L)d^5}{\rho Q^2}, \tag{2.1}$$

where (Δp) is the pressure drop across the tube, L is the length of the tube, Q is the flow rate and d is the tube diameter. Since the tube diameter is varying along the length of the tube, while the flow rate is a constant, we use a modified expression for the friction factor as

$$f = \frac{\pi^2}{8}\frac{(\Delta p/L)}{\rho Q^2}\left(\frac{1}{L}\int_0^L \mathrm{d}x\,\mathrm{d}(x)^5\right), \tag{2.2}$$

where x, the downstream distance along the tube, varies from zero to L. We use (2.2) for calculating the friction factor in the present experiments.

The instability of the laminar flow is also detected using the dye-stream method, where a dye containing coloured ink is injected at the inlet. For this purpose, a bent needle of diameter 150 μm is inserted into the centre of the conical micropipette tip at the entrance of the development section. Dye is injected into the flow at a constant flow rate using a syringe pump. Movies of the dye stream are recorded through the microscope using a Red-Lake Motion-Pro HS-4 high-speed camera, at a frame rate of 1000 frames s^{-1}. It is observed that when the flow is laminar, the dye appears as a dark cylindrical thread of diameter ∼150 μm at the centre of the tube, whereas in a turbulent flow in a rigid pipe (when the Reynolds number increases above 2100), there is the spontaneous break-up of the dye stream, as first reported by Reynolds (1893).

An experimental procedure has also been devised to detect the advent of wall oscillations. In all our experiments, there is no wall deformation observed visually in the direction perpendicular to the tube surface, and there is no visible oscillation in the wall of the tube. However, theoretical studies (Kumaran 1998*a*; Shankar & Kumaran 2001*a*) indicate that for the wall mode instability, the wall oscillation is primarily parallel to the tube surface, and it is important to detect this tangential oscillation to confirm that the instability is due to the coupling between the fluid and the wall dynamics. This detection is carried out using a He–Ne laser of power 10 mW (model number OEM5R, from Aerotech Inc.). A laser beam of diameter ∼1 mm is directed through the PDMS block along the z axis, which is perpendicular to the flow direction and microscope axis, as shown in figure 8. Owing to the difference in the refractive index between the PDMS and water, there is scattering of the laser at the tube walls. This light scattered by the tube wall is recorded using the same (Motion-Pro HS-4) high-speed camera attached to the microscope with a framing rate of 200 frames s^{-1}. It was not possible to use the maximum frame rate of 1000 frames s^{-1}, because the light requirement of the camera increases as the frame rate increases, and the intensity of the scattered light was not sufficient to measure intensity fluctuations at the maximum frame rate.

The scattered light intensity is recorded at each pixel as a function of time. The intensity at each pixel is stored as a rectangular array of dimension $1 \leqslant i \leqslant 100$ and $1 \leqslant j \leqslant 50$, where i and j are the pixel indices in the two perpendicular directions at each frame during the recording. Wall oscillations are detected by calculating the mean-square of the intensity fluctuations in time as follows. If the tube and laser are perfectly still, the intensity at each pixel, I_{ijk}, will be a constant independent of time. Here, I_{ij} is the light intensity at the pixel located at the position (i, j) in frame k. The

average intensity at each pixel, I_{ij}^{av} is then calculated as

$$I_{ij}^{av} = \frac{1}{K}\sum_{k=1}^{K} I_{ijk}, \tag{2.3}$$

where K is the total number of frames. The intensity fluctuation at pixel (i, j) in frame k are then given by

$$\Delta I_{ijk} = I_{ijk} - I_{ij}^{av}. \tag{2.4}$$

The normalized mean square of the intensity fluctuations, $\bar{I}^2$, is calculated as

$$\bar{I}^2 = \frac{\sum_{i,j}\left((1/K)\sum_{k=1}^{K}\Delta I_{ijk}^2\right)}{\sum_{i,j} I_{ij}^{av2}}. \tag{2.5}$$

As discussed above, $\bar{I}^2$ is zero if the experimental setup is perfectly stationary, since the intensity is invariant in time. In practice, there is always a small amount of vibration in the experimental setup, resulting in a non-zero value of $\bar{I}^2$. When wall oscillations are induced due to an instability, there is a sharp increase in $\bar{I}^2$, as reported in § 3.

Since the pressure gradient does deform the tube, an important question is whether the transition is due to the non-constant diameter (first diverging then converging) of the tube, or due to the wall flexibility. In order to address this issue, we fabricated a tube of non-constant diameter in hard PDMS gel with shear modulus 86.4 kPa (catalyst concentration 3 %), using a glass rod of varying diameter as the template for the test section, while the diameter is constant in the development section. The glass template was fabricated by taking a glass rod of constant diameter (1200 μm), heating it until it softens and pressing at the ends so that it bulges at the centre. By trial and error, the shape of the glass tube is adjusted so that it is as close as possible to the shape of a soft flexible tube (with gel shear modulus 17.5 kPa) deformed by an applied pressure drop. This glass tube of varying cross-section is then used as the template for forming a gel tube with varying cross-section using the procedure described above. In this manner, we fabricated a rigid tube which has the same varying diameter as a soft tube with an applied pressure drop.

If the transition is due to the variation in the cross-section of the tube, and not due to the wall flexibility, then the transition in a rigid tube of varying cross-section should occur at the same Reynolds number as that in a flexible tube of the same shape. This procedure, coupled with the observation of wall oscillations using laser scattering described above, serves to clearly establish whether the diameter variation could result in a reduction of the transition Reynolds number, or whether transition is due to wall flexibility. For the present study, we were able to fabricate a rigid tube with nearly the same diameter variation as that observed in a soft tube at a Reynolds number of 940, as shown in figure 9. The value of the $Re = 940$ was chosen, because this is the Reynolds number at which the transition in a soft tube with $G' = 17.5$ kPa occurs, as shown in the next section.

Before discussing the results, we note that the following precaution was taken to ensure that any flow disturbance due to the pressure port does not affect the results. It is well known that it takes a long distance downstream for a disturbance at the inlet of the pipe to decay even when the Reynolds number is below 2100 (Sibulkin 1962),

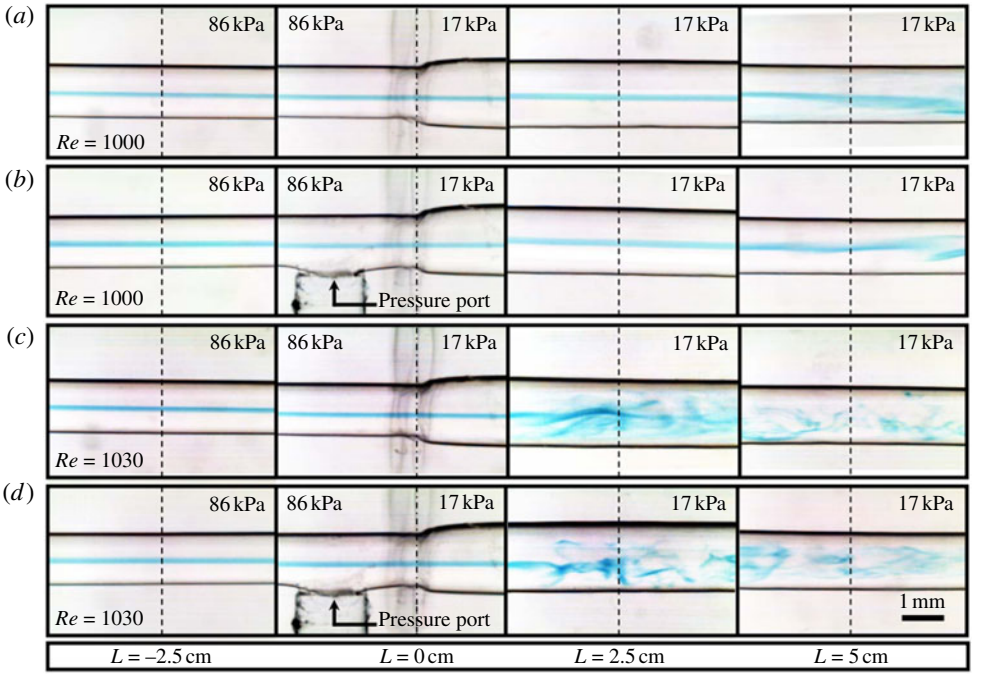

FIGURE 11. Images of the tube and the dye stream at different downstream sections in tube with diameter 1200 μm, with a development section of shear modulus 86 kPa and test section 17 kPa, without the pressure port (*a* and *c*) and with the pressure port (*b* and *d*), at Reynolds number 1000 (*a* and *b*) and Reynolds number 1030 (*c* and *d*). The transition Reynolds number is ∼950 for the soft tube with shear modulus 17 kPa. The location $L = 0$ is at the joint between the hard and soft sections.

and so it is important to verify that the flow is laminar at the entrance to the test section. First, as we had noted while discussing the fabrication of the tube, we visually examine the dye stream at the pressure port to verify that there is no disturbance. Second, when the tube is first fabricated, we first carry out dye-stream experiments before the pressure port is punched into the wall of the tube. The images of the dye stream are captured, and we record both the transition Reynolds number and the downstream location at which the dye stream becomes unstable. After this, we punch the pressure port into the wall of the tube, and carry out the experiments for the pressure drop as a function of Reynolds number. In this second series of experiments, we once again note the transition Reynolds number and the downstream location at which the dye stream becomes unstable. It is verified that the difference in the two cases is smaller than the standard deviation in the experimental measurements. An example of this is shown in figure 11, where the dye streams at different downstream sections are shown at the same Reynolds number with and without the pressure port. Clearly, there is no disturbance at the pressure port, but an instability is first observed at a location ∼5 cm from the start of the soft tube, which is more than 40 diameters downstream of the pressure port. At higher Reynolds number, the instability moves upstream to a distance of ∼2.5 cm from the start of the tube, still ∼20 diameters downstream of the pressure port. Further, the Reynolds number at which the instability is observed with the pressure port is identical, to within the standard deviation in the experiments, to the Reynolds number without the pressure port in the dye-stream

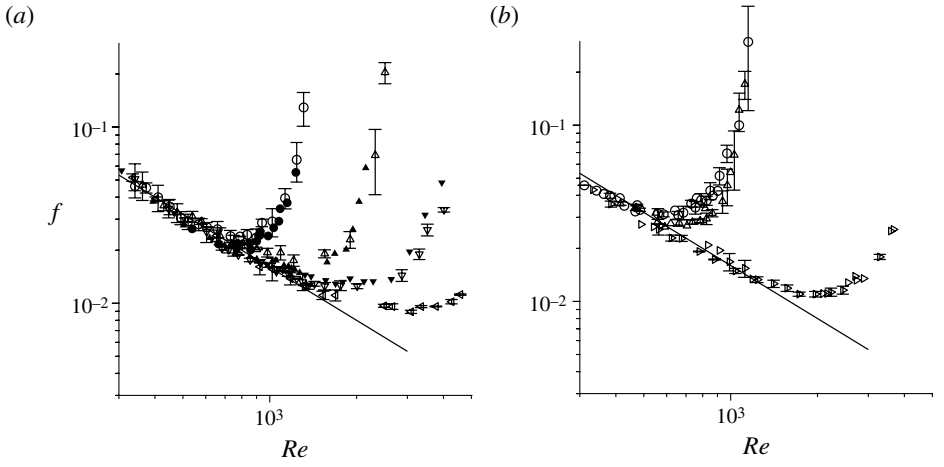

FIGURE 12. Friction factor ∘, calculated from (2.2), as a function of Reynolds number based on the average tube diameter for gel tubes with approximate diameter 1200 μm (*a*) and 800 μm (*b*), with different shear modulus and percentage of cross-linker: ∘, $G' = 17.5$ kPa, catalyst 1.75 %; △, $G' = 25.1$ kPa, catalyst 2 %; ▽, $G' = 38.0$ kPa, catalyst 2.25 %; ▷, $G' = 86.4$ kPa, catalyst 3 %. The filled symbols in (*a*) show the results for a tube with development section of length 10 cm, while the open symbols with error bars show the results for development section of length 4.5 cm. In (*b*), the development section for the 800 μm tube is 4.5 cm in length.

experiments, as shown in figure 11. This proves that the flow disturbance is not due to the presence of the pressure port.

3. Results

The friction factor is shown as a function of the Reynolds number in figure 12. At low Reynolds number, the friction factor is well described by the equation $f = 16/Re$ for a pipe flow. However, as the Reynolds number increases, there is a departure from $16/Re$. It is observed that when the gel is sufficiently hard (with cross-linker concentration of 3 %), the Reynolds number for the transition is close to 2100, which is the Reynolds number for a rigid tube. However, as the wall is made softer, the Reynolds number for transition decreases to a minimum of ∼500 for the 800 μm tubes made of the softest gels (of shear modulus ∼17 kPa).

Coinciding with the increase in the friction factor from its laminar value, we also observe an instability in the dye stream introduced at the centre of the tube. The dye stream is shown in figure 13(*a*) for three different values of the Reynolds number for a gel with 1.75 % catalyst concentration corresponding to a shear modulus of 17.53 kPa. Below the transition Reynolds number ($Re = 880$), the dye stream is perfectly straight, whereas just above the transition Reynolds number ($Re = 940$), cross-stream motion in the form of waves of a well-defined frequency are observed in the dye stream. When the Reynolds number is further increased to $Re = 1100$, we see a complete breakup of the dye stream and significant cross-stream mixing. This instability in the dye stream is very different from that in the laminar–turbulent transition in a rigid tube, shown in figure 13(*b*). In the latter case, the dye stream is straight at $Re = 1980$, below the transition Reynolds number, but there is a spontaneous and discontinuous breakup of the dye stream at the transition at $Re = 2025$. In contrast, in the flexible tube, waves

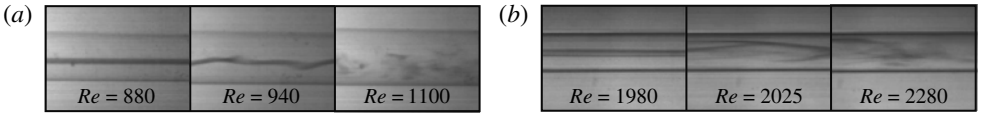

FIGURE 13. The instability observed using the dye-stream method for a tube fabricated with catalyst concentration 1.75 % ($G' = 1.753 \times 10^4$ Pa), shown at $Re = 880$, $Re = 940$ and $Re = 1100$, in (a), is contrasted with that in a rigid tube with catalyst concentration 10 % ($G' = 5.504 \times 10^5$ Pa) shown at $Re = 1980$, $Re = 2025$ and $Re = 2280$ in (b).

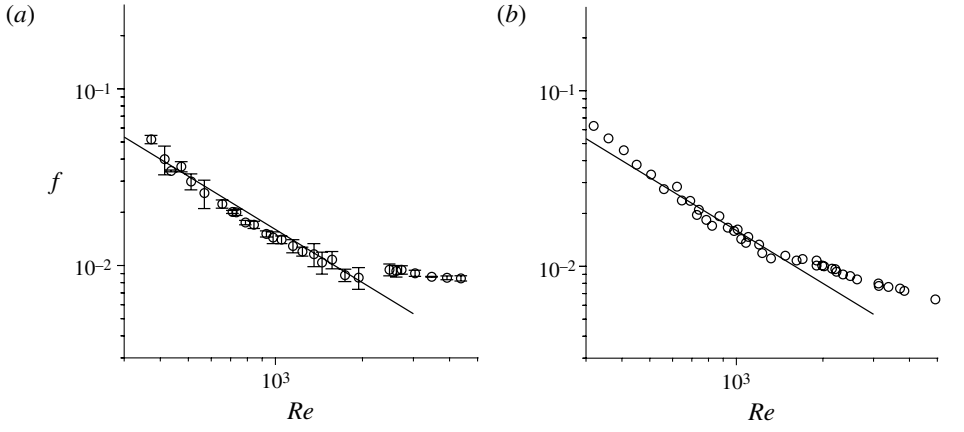

FIGURE 14. Friction factor versus Reynolds number for (a) a cylindrical gel tube fabricated with catalyst concentration 10 % ($G' = 0.55$ MPa) and diameter 1200 μm and (b) for a gel tube with varying diameter shown in figure 9, and shear modulus $G' = 0.55$ MPa.

with a well-defined frequency develop in the dye stream. The amplitude of these waves increases continuously from zero as the Reynolds number is increased, and breakup occurs when the amplitude becomes ∼20 % of the tube radius.

There is also a qualitative difference in the friction factor at transition in hard and soft gels, as shown in figure 14(a). For the cylindrical tube with shear modulus 0.55 MPa, it is observed in figure 14(a) that the flow is laminar up to a Reynolds number of 2000, and then there is a discontinuity at transition. It is difficult to obtain data very close to transition, because we are maintaining the flow rate using a needle valve and measuring pressure drop, and control of the flow rate becomes difficult close to the transition Reynolds number. However, the data both at $Re = 2000$ and $Re = 2300$ is consistent with a discontinuity in the friction factor.

We have conducted one other test to show that the instability is due to the wall flexibility, and not due to tube deformation. As explained in the previous section, a tube of varying diameter but with shear modulus 0.55 MPa, shown by the dashed line in figure 9, was fabricated to mimic, as closely as possible, the tube shape at the transition Reynolds number of ∼940 for a soft tube with shear modulus 17.53 kPa. The variation of friction factor with Reynolds number for this tube, shown in figure 14(b) is qualitatively different from that for soft tubes shown in figure 12. This is conclusive evidence that the instability is not due to the change in shape of the tube alone, but is due to the flexibility of the walls of the tube. Images of the flow through the tube of varying cross-section are shown in figure 15. Figure 15(a)–(c),

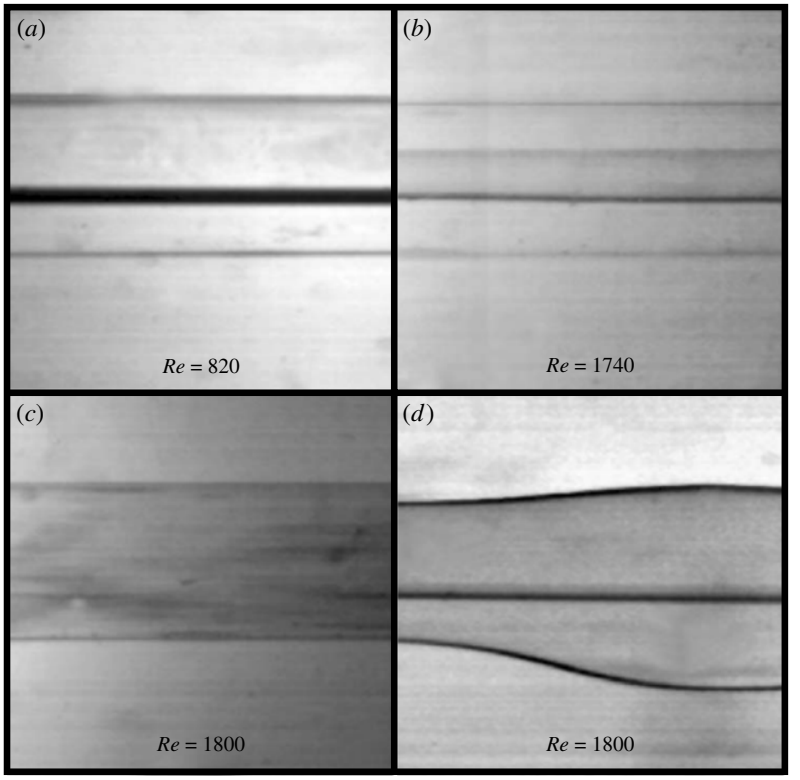

FIGURE 15. The dye stream at a location 3.5 cm downstream from the tube entrance at different Reynolds numbers (*a*), (*b*) and (*c*), and at the entrance of the tube at an average Reynolds number of 1800, (*d*).

taken at a distance of 3.5 cm from the entrance of the tube, clearly show that there is an instability only when the Reynolds number based on the average tube diameter is ∼1800. At the transition point, the Reynolds number based on the local diameter is 2050, because the local diameter at a distance 3.5 cm from the entrance is smaller than the average diameter. This clearly indicates that the transition in the tube of varying diameter is identical to the rigid-tube transition based on the local Reynolds number. When transition takes place at $Re = 1800$ (based on average diameter) at the distance 3.5 cm from the entrance, the flow in the expanded section is undisturbed, as shown in figure 15(*d*). This clearly shows that the transition is not due to tube expansion.

Owing to the variation in the tube diameter, there is a variation in the Reynolds number along the tube length, and the pressure gradient is not a constant. This could raise a concern that the Reynolds number at some axial locations could be higher than the rigid tube transition Reynolds number. In order to allay this concern, we have plotted the local Reynolds number as a function of axial position along the tube in figure 16 for the flexible tubes of diameter 1200 μm just before transition. Here, the local mean velocity is calculated as the ratio of the flow rate and the cross-sectional area, and the Reynolds number is calculated using the diameter and mean velocity. Although there is an approximation that the local velocity is parabolic in this calculation, it still provides an estimate of the variation in the Reynolds number due to the variation in tube diameter. Figure 16 clearly shows that the variation in the tube diameter does not increase the local Reynolds number to the rigid-tube transition

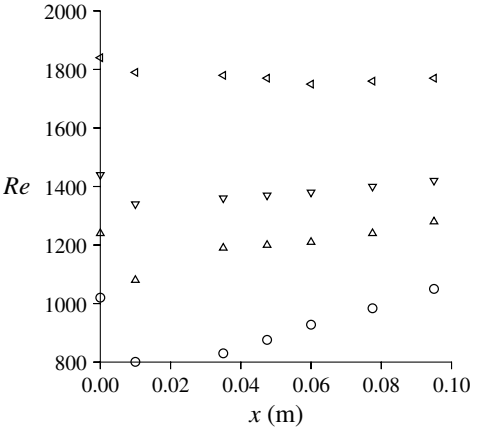

FIGURE 16. Reynolds number based on the local mean velocity and diameter as a function of downstream distance from the start of the soft tube for gel tubes with approximate diameter 1200 μm and with different shear modulus and percentage of cross-linker: ○, $G' = 17.5$ kPa, catalyst 1.75 %, average Reynolds number 890; △, $G' = 25.1$ kPa, catalyst 2 %, average Reynolds number 1190; ▽, $G' = 38.0$ kPa, catalyst 2.25 %, average Reynolds number 1373; ◁, $G' = 86.4$ kPa, catalyst 3 %, average Reynolds number 1780.

value, and the transition takes place even when the maximum local Reynolds number is approximately half the transition value in rigid tubes for the lowest shear modulus used here.

The laser scattering technique was used to determine the onset of wall oscillations in the experiments. The mean-square intensity $\bar{I}^2$ (2.5) is shown as a function of Reynolds number in figure 17. The laser amplitude exhibits small variations due to the input alternating voltage, and consequently there is a non-zero mean-square intensity even in the absence of flow. The absolute value of the mean-square intensity varies in the different experiments because it depends on the alignment of the laser with respect to the gel, and the irregularities in each individual gel sample which results in laser scattering. However, in all cases, it is observed that the transition is accompanied by a sharp increase of approximately an order of magnitude in the normalized mean-square intensity $\bar{I}^2$ (see (2.5)), indicating the onset of oscillations in the wall material. As shown in figure 17, the Reynolds number for the onset of oscillations depends on the hardness of the gel. For gels with a large shear modulus (3 % catalyst concentration), there is no sharp transition in $\bar{I}^2$ at the laminar–turbulent transition Reynolds number of 2100, even though the friction factor in figure 12, as well as in the dye-stream experiments, indicates that a transition has taken place. However, for soft gels with catalyst concentration less than 2.5 %, there is a sharp increase in $\bar{I}^2$ coinciding with the increase in the friction factor in figure 12. This indicates that the onset of wall oscillations does take place at the Reynolds number where the flow becomes unstable. Visually, we observe a rapid flickering in the image at the transition point, indicating that the wall is oscillating.

The Reynolds number for the instability in the dye stream (figure 13) and the Reynolds number for the onset of wall oscillations (figure 17) and the transition Reynolds number where the friction factor departs from the laminar value (figure 12) are shown in figure 18(*a*). It is clear that subject to error bars, the transition Reynolds number from the friction factor measurements is identical to the Reynolds number for

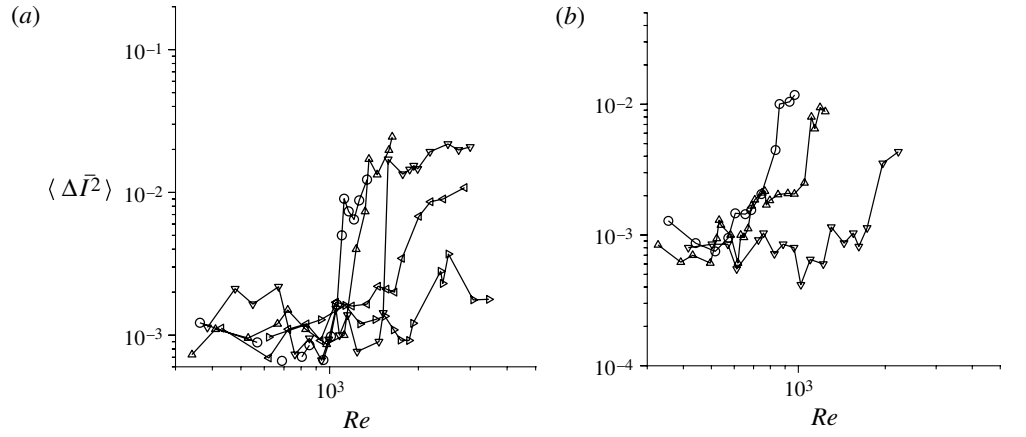

FIGURE 17. The intensity $\bar{I}^2$, (2.5) as a function of Reynolds number for tube diameter $\sim$1200 μm (*a*) and 800 μm (*b*) for gels with different shear modulus and percentage of cross-linker, $\circ\ G' = 1.753 \times 10^4$ Pa, catalyst 1.75 %, $\triangle\ G' = 2.507 \times 10^4$ Pa, catalyst 2 %, $\nabla\ G' = 3.800 \times 10^4$ Pa, catalyst 2.25 %, $\triangleleft\ G' = 5.438 \times 10^4$ Pa, catalyst 2.5 %, $\triangleright\ G' = 8.639 \times 10^4$ Pa, catalyst 3 %.

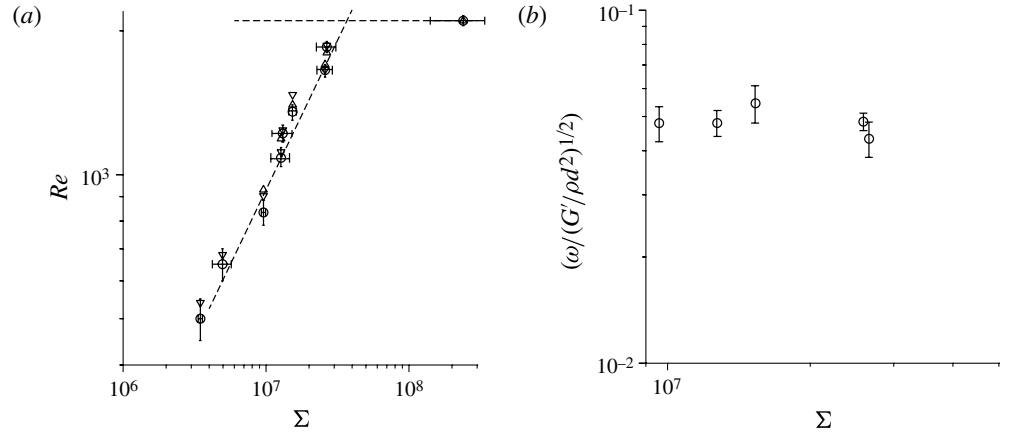

FIGURE 18. Transition Reynolds number (*a*) and the scaled frequency of oscillations $(\omega/(G'/\rho d^2)^{1/2})$ from the dye-stream experiments (*b*) as a function of the parameter $\Sigma = (\rho G R^2/\eta^2)$. In (*a*), the different symbols represent the transition Reynolds number obtained from the friction factor ∘, the dye-stream method (△) and the onset of wall oscillations (∇), and the line shows the power law $\Sigma^{5/8}$.

the advent of oscillations in the dye stream and oscillations in the wall of the tube. This shows that the transition is due to wall oscillations induced by the dynamical coupling between the fluid flow and the wall dynamics.

Figure 12 shows the continuous increase in the friction factor at the transition point. It is also apparent from the dye-stream experiments that there is a continuous increase in the oscillation amplitude at the transition point, as shown in figure 13. This is different from the transition in a rigid tube, where there is a discontinuous break up of the dye stream at transition. We have attempted to measure the amplitude of the waves (one-half of the separation between the crest and trough) of the dye stream

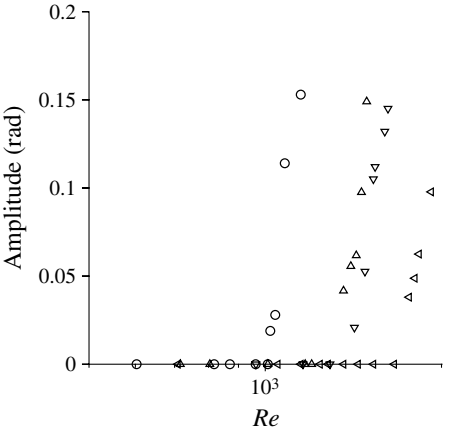

FIGURE 19. Amplitude of the waves in the dye stream, scaled by the tube radius, at a location 5 cm downstream from the start of the flexible section of the tube, as a function of the average Reynolds number for gel tubes with approximate diameter 1200 μm and with different shear modulus and percentage of cross-linker: ○, $G' = 17.5$ kPa, catalyst 1.75 %; △, $G' = 25.1$ kPa, catalyst 2 %; ▽, $G' = 38.0$ kPa, catalyst 2.25 %; ◁, $G' = 54.4$ kPa, catalyst 2.5 %.

as a function of the Reynolds number close to transition, using image processing. Figure 19 shows the ratio of the amplitude and the radius of the tube at a location 5 cm downstream from the inlet of the soft section. The minimum amplitude that could be detected is as low as 0.02 times the tube radius for the softest tube used here, and we are able to capture a continuous increase in the amplitude as the Reynolds number is increased, until the break up of the dye stream when the amplitude reaches ∼20 % of the tube radius. This result, along with the continuous increase in friction factor at transition in figure 12, lead us to conclude that the transition in a flexible tube is a continuous transition, which is qualitatively different from the discontinuous transition in a rigid tube.

The frequency of oscillations can be measured in the dye-stream experiments from the images by measuring the radial displacement of the dye in time at a fixed cross-section of the tube, as shown in figure 13. The video of the time evolution of the dye stream is recorded with a Red Lake Motion-Pro high-speed camera at a framing rate of 1000 frames s^{-1}. From this, the time period and frequency of oscillation are extracted by locating the radial position of the dye stream at a fixed stream-wise location, and measuring the time taken for the oscillation of the dye stream. This frequency was calculated for the tube with approximate diameter 1200 μm; as noted earlier, we were not able to carry out dye-stream experiments for the tube with approximate diameter 800 μm. The theoretical analysis (Shankar & Kumaran 2001*a*, 2002) predicts that the frequency of oscillations should be of the order of 100–500 Hz. In our experiments, we find the frequency to be in the same range. The theory further predicts that the frequency increases proportional to $(G/\rho d^2)^{1/2}$ as the shear modulus increases. The results in figure 18(*b*) are consistent with this scaling relation, subject to error bars in the frequency measurements.

Figure 18(*a*) also shows that the power law $Re \propto \Sigma^{5/8}$ best fits the data. This is slightly different from the power law $Re \propto \Sigma^{3/4}$ expected for the wall mode instability. Further, the transition Reynolds number is much smaller than that predicted for the wall mode instability. The reasons for this are discussed in the next section.

4. Discussion

Recent work (Sharp & Adrian 2004; Rands, Webb & Maynes 2006), both based on friction factor measurements as well as micro-PIV, has shown that the transition in rigid microtubes with diameter as low as 57 μm is no different from that in conventional pipe flows. All of the precautions taken in this study also clearly show that the transition in a sufficiently hard tube takes place at a Reynolds number of ∼2000, and the qualitative nature of the transition is no different from that in rigid tubes. Therefore, the anomalous transition observed here is due to wall flexibility alone, and cannot be attributed to the dimensions of the tube.

The transition Reynolds number, shown in figure 18(*a*), follows the empirical relation $Re_t = 0.0392\Sigma^{5/8}$. This is much smaller than the transition Reynolds number in the experiments of Krindel & Silberberg (1979), which were carried out in gel tubes with diameter 0.13 mm, and two values of the gel shear modulus, 1.2 and 0.3 kPa. For these values of the shear modulus, the parameter Σ is 2.7×10^4 and 6.75×10^3, respectively. The corresponding transition Reynolds numbers predicted by the correlation $Re_t = 0.0392\Sigma^{5/8}$ are ∼23 and 10, respectively. In contrast, Krindel and Silberberg reported transition Reynolds numbers of 570 and 870 for the two gels. Thus, it appears that the present instability mechanism is qualitatively different from that reported by Krindel & Silberberg (1979). The transition Reynolds number is also much smaller than the theoretical prediction for the wall mode instability (Shankar & Kumaran 2002). The theoretical transition Reynolds number is $\sim 6 \times 10^3$ at $\Sigma = 10^6$, and $\sim 3.2 \times 10^4$ at $\Sigma = 10^7$. However, the scaling $Re_t \propto \Sigma^{5/8}$ is close to the prediction of $Re_t \propto \Sigma^{3/4}$ for the wall mode instability. This scaling, coupled with the observation of significant tangential wall motion but very little motion normal to the wall, suggests that this instability is a wall mode instability, but one which is significantly modified by the wall deformation due to the applied pressure gradient.

The wall mode instability is a high Reynolds number instability, where the viscous effects are comparable to inertial effects in a 'wall layer' of thickness $Re^{-1/3}$ at the wall. This instability is driven by the transport of energy from the mean flow to the fluctuations due to the shear work done by the mean flow in the wall layer. The velocity perturbations exhibit unusual scalings in the wall layer (Shankar & Kumaran 2001*a*,*b*), very different from those in usual boundary layer theories. If $\tilde{v}_x$ is the streamwise velocity in the wall layer at the wall of the tube, then the cross-stream velocity (in the radial direction) scales as $\tilde{u}_r \sim Re^{-1/3}\tilde{v}_x$. In the flexible wall, the displacement fields in the stream-wise and cross-stream directions, $\tilde{u}_x$ and $\tilde{u}_r$, are comparable in magnitude. The continuity of velocity and continuity of stress conditions are applied at the interface between the fluid and the flexible wall. The high Reynolds number asymptotic analysis (Shankar & Kumaran 2001*a*,*b*) indicates that it is appropriate to apply zero normal displacement conditions ($\tilde{u}_r = 0$) and zero shear stress conditions $\tilde{\sigma}_{xr} = 0$ at the interface between the fluid and the flexible surface. This is the required matching condition, because the magnitude of the stress and velocity in the fluid is small compared with that within the viscoelastic solid surface in the limit $Re \gg 1$. This scaling is in agreement with our experimental observations; the microscope images show very little motion normal to the surface of the gel tube, even when there significant motion is detected within the gel by the laser scattering technique.

While further work needs to be done to examine why the experimental transition Reynolds number is an order of magnitude lower than the theoretical prediction, we can explain the difference in the scaling of the transition Reynolds number with the parameter Σ. The transition Reynolds number in Shankar & Kumaran (2000, 2001*a*,*b*)

was calculated for a parabolic velocity profile. However, the flow in a converging tube is much flatter than the parabolic profile (Sutterby 1965; Shankar & Kumaran 1999), and the velocity gradient at the wall is higher than the value of $(2U_{max}/R)$ for a parabolic flow, where U_{max} is the maximum velocity and R is the tube radius. If α is the slope of the tube wall, there is a significant departure from a parabolic profile when $Re\,\alpha > 1$, even when the slope α is small. In the limit $Re\,\alpha \gg 1$, simple boundary layer analysis indicates that the velocity profile is close to a plug flow in the centre of the tube, and viscous effects are important within a region of thickness $(Re\,\alpha)^{-1/2}$ at the wall. Therefore, the strain rate at the wall scales as $(Re\,\alpha)^{1/2}(U_{max}/R)$.

Since the strain rate at the wall in a converging tube is $(Re\,\alpha)^{1/2}$ higher than that for a parabolic flow for $Re\,\alpha \gg 1$, we would expect the transition Reynolds number in a converging tube, based on the maximum velocity and tube radius, to be $O(Re\,\alpha)^{-1/2}$ smaller than that for a parabolic flow. The slope α can be estimated as follows. The pressure gradient across the ends of the tube increases proportional to the coefficient of viscosity and the flow velocity. The resistance to deformation within the wall increases proportional to the shear modulus G. Just from dimensional analysis, it is easy to see that the dimensionless slope α has to be proportional to $(U_{max}\eta/GR) \sim (Re/\Sigma)$, provided that the tube wall is considered of infinite thickness so that the only length scale is the tube radius R. From, this, we find that $(Re\,\alpha) \sim (Re^2/\Sigma)$. The transition Reynolds number for an undeformed tube scales proportional to $\Sigma^{3/4}$ for the wall mode, the transition Reynolds number for the deformed is $Re_t \propto (Re_t\alpha)^{-1/2}\Sigma^{3/4} \propto (Re_t^2/\Sigma)^{-1/2}\Sigma^{3/4}$. From this, we find the experimental scaling, $Re_t \propto \Sigma^{5/8}$.

The experimental result obtained here, that the transition Reynolds number is much lower than that predicted previously, opens up a significant opportunity for using this instability to induce mixing in microfluidic applications. For a gel of shear modulus 10^4 Pa and a fluid with viscosity 10^{-3} kg m^{-1} s^{-1}, the transition Reynolds number is ~850 for a 1 mm diameter tube, but decreases to 25 for a 100 μm diameter tube and 0.84 for a 10 μm diameter tube. In contrast, the scaling laws of previous theoretical studies (Kumaran 1998*b*; Shankar & Kumaran 2002) predict that the transition Reynolds number is ~40 times higher at the same value of Σ. The mean velocities required for the instability, 0.8 m s^{-1} for a 1 mm tube and 0.25 m s^{-1} for a 100 μm tube, and 8 cm s^{-1} for a 10 μm tube, are relatively large, but achievable in practice. In fact, the enhanced mixing due to the instability would compensate for the shorter residence time at a higher flow rate. Thus, our experiments have shown that it is practically feasible to use soft walls to induce an instability and generate mixing in microfluidic applications.

The authors would like to thank the Department of Science and Technology, Government of India for financial support. It is an honour to contribute this article to the *Festschrift* for Professor T. J. Pedley. For many years, Professor Pedley has provided constant encouragement to those of us working in the broad area of bio-fluid dynamics with his insight and his inimitable sense of humour.

REFERENCES

BAZANT, M. Z. & SQUIRES, T. M. 2004 Induced-charge electro-kinetic phenomena: theory and microfluidic applications. *Phys. Rev. Lett.* **92**, 066101.

CHANDRASEKHAR, S. 1981 *Hydrodynamic and Hydromagnetic Stability*. Dover Publications Inc.

CHOKSHI, P. P. & KUMARAN, V. 2008 Weakly nonlinear analysis of viscous instability in flow past a neo-Hookean surface. *Phys. Rev.* E **77**, 056303.

CHOKSHI, P. P. & KUMARAN, V. 2009 Weakly nonlinear stability analysis of a flow past a neo-Hookean solid at arbitrary Reynolds numbers. *Phys. Fluids* **21**, 014109.

DRAZIN, P. G. & REID, W. H. 1981 *Hydrodynamic Stability*. Cambridge University Press.

EGGERT, M. D. & KUMAR, S. 2004 Observations of instability, hysteresis, and oscillation in low-Reynolds-number flow past polymer gels. *J. Colloid. Interface Sci.* **278**, 234–242.

GAURAV & SHANKAR, V. 2009 Stability of fluid flow through deformable neo-Hookean tubes. *J. Fluid Mech.* **627**, 291–322.

HOF, B., JUEL, A. & MULLIN, T. 2003 Scaling of the turbulence transition threshold in a pipe. *Phys. Rev. Lett.* **91**, 244502.

HOF, B., WESTERWEEL, J., SCHNEIDER, T. M. & ECKHARDT, B. 2006 Finite lifetime of turbulence in shear flows. *Nature* **443**, 59–62.

KERSWELL, R. R. 2005 Recent progress in understanding the transition to turbulence in a pipe. *Nonlinearity* **18**, R17–R44.

KRINDEL, P. & SILBERBERG, A. 1979 Flow through gel-walled tubes. *J. Colloid. Interface Sci.* **71**, 39–50.

KUMARAN, V. 1995 Stability of the viscous flow of a fluid through a flexible tube. *J. Fluid Mech.* **294**, 259–281.

KUMARAN, V. 1996 Stability of an inviscid flow in a flexible tube. *J. Fluid Mech.* **320**, 1–17.

KUMARAN, V. 1998*a* Stability of wall modes in a flexible tube. *J. Fluid Mech.* **362**, 1–15.

KUMARAN, V. 1998*b* Stability of fluid flow in a flexible tube at intermediate Reynolds number. *J. Fluid Mech.* **357**, 123–140.

KUMARAN, V. 2003 Hydrodynamic stability of flow through flexible channels and tubes. In *Flow Through Collapsible Tubes and Past Other Highly Compliant Surfaces* (ed. P. W. Carpenter & T. J. Pedley). Kluwer Academic.

KUMARAN, V., FREDRICKSON, G. H. & PINCUS, P. 1994 Flow induced instability at the interface between a fluid and a gel at low Reynolds number. *J. Phys. France* II **4**, 893–911.

KUMARAN, V. & MURALIKRISHNAN, R. 2000 Spontaneous growth of fluctuations in the viscous flow of a fluid past a soft interface. *Phys. Rev. Lett.* **84**, 3310–3313.

LEE, J. N., PARK, C. & WHITESIDES, G. M. 2003 Solvent compatibility of poly (dimethyl siloxane) based microfluidic devices. *Analyt. Chem.* **75**, 6544–6553.

MURALIKRISHNAN, R. & KUMARAN, V. 2002 Experimental study of the instability of the viscous flow past a flexible surface. *Phys. Fluids* **14**, 775.

RANDS, C., WEBB, B. W. & MAYNES, D. 2006 Characterisation of transition to turbulence in microchannels. *Intl J. Heat Mass Transfer* **49**, 2924–2930.

REYNOLDS, O. 1893 An experimental investigation of the circumstances which determine whether the motion of water in parallel channels shall be direct or sinuous and of the law of resistance in parallel channels. *Phil. Trans. R. Soc.* **174**, 935.

SHANKAR, V. & KUMARAN, V. 1999 Stability of non-parabolic flows in a flexible tube. *J. Fluid Mech.* **395**, 211–236.

SHANKAR, V. & KUMARAN, V. 2000 Stability of non-axisymmetric modes in a flexible tube. *J. Fluid Mech.* **407**, 291–314.

SHANKAR, V. & KUMARAN, V. 2001*a* Asymptotic analysis of wall modes in a flexible tube revisited. *Eur. Phys. J.* B **19**, 607.

SHANKAR, V. & KUMARAN, V. 2001*b* Weakly nonlinear stability of viscous flow past a flexible surface. *J. Fluid Mech.* **434**, 337–354.

SHANKAR, V. & KUMARAN, V. 2002 Stability of wall modes in the flow past a flexible surface. *Phys. Fluids* **14**, 2324.

SHARP, K. V. & ADRIAN, A. J. 2004 Transition from laminar to turbulent flow in liquid filled microtubes. *Exp. Fluids* 741–747.

SHRIVASTAVA, A., CUSSLER, E. L. & KUMAR, S. 2008 Mass transfer enhancement due to a soft elastic boundary. *Chem. Engng Sci.* **63**, 4302–4305.

SIBULKIN, A. 1962 Transition from turbulent to laminar pipe flow. *Phys. Fluids* **5**, 280–284.

STROOCK, A. D., DERTINGER, S. K. W., AJDARI, A., MEZIC, I., STONE, H. A. & WHITESIDES, G. M. 2002 Chaotic mixer for microchannels. *Nature* **295**, 647–651.

SUTTERBY, J. L. 1965 Finite difference analysis of viscous laminar converging flow in conical tubes. *Appl. Sci. Res.* A **15**, 241–252.

THAOKAR, R. M., SHANKAR, V. & KUMARAN, V. 2001 Effect of tangential interface motion on the viscous instability in fluid flow past flexible surfaces. *Eur. Phys. J.* B **23**, 533.

VERMA, M. K. S., MAJUMDER, A. & GHATAK, A. 2006 Embedded template-assisted fabrication of complex microchannels in PDMS and design of a microfluidic adhesive. *Langmuir* **22**, 10291–10295.

YANG, C., GRATTONI, C. A., MUGGERIDGE, A. H. & ZIMMERMAN, R. W. 2000 A model for steady laminar flow through a deformable gel-coated channel. *J. Colloid. Interface Sci.* **266**, 104–111.